ACS APPLIED MATERIALS & INTERFACES

Research Article

www.acsami.org

Investigation of Reaction Mechanisms of Bismuth Tellurium Selenide Nanomaterials for Simple Reaction Manipulation Causing Effective Adjustment of Thermoelectric Properties

Cham Kim,*[,†] Dong Hwan Kim,[†] Jong Tae Kim,[†] Yoon Soo Han,[‡] and Hoyoung Kim*[,†]

[†]Daegu Gyeongbuk Institute of Science and Technology (DGIST), 50-1 Sang-ri, Hyeonpung-myeon, Dalseong-gun, Daegu 711-873, Republic of Korea

[‡]Department of Advanced Energy Material Science and Engineering, Catholic University of Daegu, 330 Geumrak 1-ri, Hayang-eup, Gyeongsan, North Gyeongsang 712-702, Republic of Korea

Supporting Information

ABSTRACT: We synthesized ternary n-type bismuth tellurium selenide nanomaterials for thermoelectric applications via a water-based chemical reaction under an atmospheric environment. In this work, bismuth nitrate was employed as a bismuth precursor and was hydrolyzed to form bismuth hydroxide in an aqueous solution. Ascorbic acid was used to dissolve the bismuth hydroxide and give a reactive bismuth source (Bi^{3+} ions) that was able to react with anion sources (Te^{2-}/Se^{2-} ions). Ascorbic acid played a role in reducing bismuth hydroxide to an unreactive bismuth source (bismuth particles, Bi^0). We confirmed that ascorbic acid dissolved or reduced bismuth hydroxide depending on the solution pH. Because either Bi^{3+} ions or bismuth particles were generated depending on the pH, the nanomaterial stoichiometry was pH dependent. Nanomaterials prepared at various pH levels were individually sintered using a spark plasma sintering process to measure their thermoelectric transport properties (i.e., carrier concentration, electrical resistivity, Seebeck coefficient, and thermal conductivity). We observed how the transport properties were affected through adjustment of the pH of the reaction and found an appropriate pH for optimizing the transport properties, which resulted in enhancement of the thermoelectric performance.

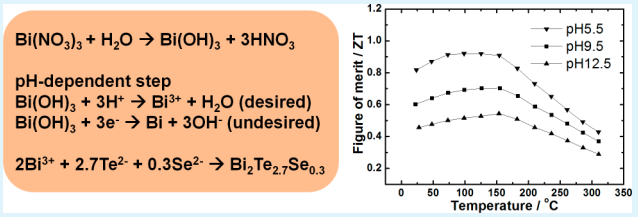

KEYWORDS: *thermoelectric materials, transport properties, bismuth tellurium selenide, chemical reaction, pH value*

1. INTRODUCTION

Thermoelectric technology has been intensively investigated due to its attractive applications, which include heat-to-electricity conversion and solid-state cooling.[1−7] Thermoelectric power generation is a promising technology for the conversion of exhaust heat, which is emitted in the automotive and steel industries, into electricity. Thermoelectric cooling is a cooling technology that is applicable to microelectronics, infrared detectors, and optoelectronics. However, a wide range of thermoelectric applications has been restricted due to the low energy conversion efficiency of current thermoelectric materials.[8−10] The comprehensive performance of such materials is evaluated via the dimensionless figure of merit ZT ($= \alpha^2\sigma T/\kappa$), where α is the Seebeck coefficient, σ is the electrical conductivity, T is the absolute temperature, and κ is the thermal conductivity.[5−7,11−13] To obtain an excellent thermoelectric material, a high ZT value should be guaranteed through enhancement of the power factor ($\alpha^2\sigma$) or reduction of the thermal conductivity (κ).[8,9,14−23]

With the meteoric development in nanotechnology, numerous researchers have intensively concentrated on building various nanomaterials to realize such unique and attractive characteristics in low dimensional structures as quantum confinement and phonon scattering effects.[24−28] Basically, thermoelectric researchers are highly interested in low dimensional structures because they can accomplish high $\alpha^2\sigma$ and low κ from the effects, simultaneously. Reports have revealed that ZT can remarkably be enhanced in low dimensional structures such as quantum dots (QD) and superlattice (SL) thin films both because of the increase in the power factor ($\alpha^2\sigma$) and the decrease in κ.[15−23] However, the commercial use of these substances is difficult because of complicated production processes and high costs. Therefore, many thermoelectric researchers have intensively examined synthetic methodologies for the preparation of nanomaterials in bulk phases such as nanoparticles,[29−31] nanotubes,[32−34] and nanowires.[35−37] These bulk-phase methods may result in reduced thermal conductivity caused by phonon scattering in nanostructures and can facilitate scale-up and commercialization due to relatively brief fabrication processes and low expenses. TE materials are usually classified according to the temperatures at which they are operated. For low-temperature operations (0 to 300 °C), a representative material is a Bi_2Te_3-based compound. The material includes specific nanoscale

Received: April 8, 2013
Accepted: December 29, 2013
Published: December 29, 2013

structures such as nanograins of $Bi_xSb_{2-x}Te_3$ alloy[31,38] and bulk composites laminated by a nanosized BiSbTe alloy.[39] Research into Bi_2Te_3-based nanobulk materials has mostly been based on the p-type semiconductor $Bi_xSb_{2-x}Te_3$ because of its high power factor.[16,40−44] Nanobulk $Bi_xSb_{2-x}Te_3$ materials are known to exhibit excellent ZT values as high as ∼1.5[31,39] because of the synergetic effect between the high power factor and the low thermal conductivity.

Both p-type and n-type materials are required for the creation of thermoelectric modules; however, n-type Bi_2Te_3-based nanobulk materials still show relatively low ZT values, likely because of their low power factors.[45,46] Consequently, n-type Bi_2Te_3-based nanobulk materials with outstanding thermoelectric performance should be developed. Our group has worked to develop an n-type $Bi_2Te_{2.7}Se_{0.3}$ nanobulk material. In our previous work, we synthesized a $Bi_2Te_{2.7}Se_{0.3}$ nanomaterial via a water-based solution process.[45,47] Precursors of each element were individually dissolved in an aqueous solution using chemical additives, and reactive cations (Bi^{3+} ions) and anions (Te^{2-}/Se^{2-} ions) were obtained. These ions were reacted to obtain a $Bi_2Te_{2.7}Se_{0.3}$ nanopowder that was sintered via a spark plasma sintering process to produce a bulk phase with a small degree of grain growth. The resulting $Bi_2Te_{2.7}Se_{0.3}$ nanobulk material exhibited a much lower thermal conductivity compared to that of the single-crystalline equivalent. However, the nanobulk material mostly showed a high carrier concentration, which resulted in a low Seebeck coefficient and a poor power factor. The nanobulk material exhibited a low ZT value because the negative effect of the low power factor in the nanobulk material overwhelmed the benefit of the low thermal conductivity. We proved that the high carrier concentration of the nanobulk material resulted from the lower-than-intended bismuth ratio. In the present study, we examined why the bismuth ratio was lower than intended and confirmed that it resulted from a loss of the reactive bismuth source (i.e., Bi^{3+} ions) due to the pH of the aqueous solution used in the synthesis. Accordingly, we performed the reaction while varying the pH and closely observed the stoichiometric variations. The bismuth ratio was pH dependent, and thus, the transport properties of the product (i.e., its carrier concentration, electrical resistivity, Seebeck coefficient, and thermal conductivity) should also vary with the pH level. Specifically, we could optimize the transport properties of our $Bi_2Te_{2.7}Se_{0.3}$ nanobulk material by adjusting the reaction conditions, which led to enhanced ZT values.

2. EXPERIMENTAL SECTION

2.1. Chemicals. Bismuth(III) nitrate ($Bi(NO_3)_3$, Kojundo Chemical, 99.99%) and elemental tellurium/selenium powders (Te/Se, Kojundo Chemical, 99.999%, 45 μm) served as precursors. Ascorbic acid ($C_6H_8O_6$, Junsei Chemicals, 99%) and ethylenediaminetetraacetic acid (EDTA: $C_{10}H_{16}N_2O_8$, Junsei Chemicals, 99.4%) were used to dissolve the bismuth precursor and to stabilize it in deionized water. 5.0 M Sodium hydroxide aqueous solution was prepared by using sodium hydroxide beads (NaOH, Daejung, 97%) to adjust pH. Sodium borohydride ($NaBH_4$, Samchun, 99%) was used to reduce the Te and Se powders. All chemicals were used without further purification.

2.2. Sample Preparation. 60 mmol of bismuth nitrate was mixed with 200 mL of deionized water, and 30 mmol of both ascorbic acid and EDTA were subsequently added. The resulting pale-yellow suspension was vigorously stirred until it reached a stable pH of 1.5. A solution of NaOH (5.0 M) was slowly added to the mixture to adjust the pH to greater than 2.5, at which point a yellow, cloudy solution without undissolved particles was obtained. This solution became completely transparent after it was stirred for an additional ca. 3 h. The solution was colorless at pH values from 3 to 5 but became transparent pale-yellow at pH levels from 6 to 8. When we increased the pH further, the solution became dark-orange or brown (pH 9 to 11) and finally changed to black (pH > 12). We prepared three solutions with different pH values (i.e., pH 5.5, 9.5, and 12.5) and labeled them "A solutions". Meanwhile, 81 mmol of Te and 9 mmol of Se were placed in a three-neck round-bottom flask, and the flask was purged with N_2. Then, 250 mL of 0.3 M $NaBH_4$ aqueous solution was added. This Te and Se mixture was heated to 100 °C with vigorous stirring. When the mixture became a transparent purple solution, the three different A solutions were individually added. A black precipitate instantly appeared and was refluxed for 48 h. The precipitate was filtered and rinsed thoroughly using dry ethanol and deionized water. After the precipitate was dried under vacuum at 60 °C overnight, a black powder was obtained. The resulting powder was sintered with spark plasma sintering equipment (SPS; DR. Sinter, SPS-3, 20MK-IV) at 350 °C under a pressure of 50 MPa in an Ar atmosphere. The heating rate was 80 K min^{-1}, and the holding time at this sintering temperature was 2 min.

2.3. Characterization Studies. Dynamic light scattering (DLS; Brookhaven Instruments Company photon correlation spectrometer equipped with a BI-200SM goniometer and a BI-9000AT correlator) measurements were performed to analyze the size of the bismuth sources stabilized in the A solutions. Measurements of chemical composition were performed on an inductively coupled plasma mass spectrometry (ICP-MS, Perkin-Elmer Norwalk, CT). Electron-backscatter diffraction (EBSD) analysis was conducted with a Hitachi S-4300SE scanning electron microscope. The scan area was 30 × 30 μm^2, and a step size of 0.05 μm was used at an accelerating voltage of 25 kV. The EBSD sample was prepared via mechanical and vibrational polishing in an aqueous solution that contained the colloidal silica particles. Powder X-ray diffraction (XRD) patterns were collected with a D/MAX-2500 diffractometer (Rigaku) using Cu Kα radiation (λ = 1.5406 Å) and a scintillation counter detector. Crystal structures were confirmed and refined using the powder profile refinement program GSAS.[48] The electrical resistivity (ρ) and Seebeck coefficient (α) were measured simultaneously with an LSR-3 instrument (Linseis Thermal Analysis). The carrier mobility (μ) was calculated with the equation: $\mu = 1/(\rho ne)$, where e is electric charge, 1.6×10^{-19} C. The carrier concentration (n) was measured using an HL5500PC-M (Bio-Rad) Hall-effect measurement system. The thermal conductivity (κ) is related to the thermal diffusivity (λ) through the equation $\kappa = \lambda C_p d$, where d and C_p denote the density and specific heat of the sample, respectively. The thermal diffusivities of the samples between 300 and 573 K were measured with a laser flash tool (LFA447, Netzsch). The density was approximately 98% of the theoretical density for a Bi_2Te_3 bulk material, 7.878 g cm^{-3}.[16] We measured the specific heat capacity using a differential scanning calorimeter (DSC200, Netzsch). We adopted the measured values of λ and C_p to calculate the thermal conductivity using the previously stated equation. The thermal conductivity is roughly determined by the sum of carrier thermal conductivity (κ_e) and lattice thermal conductivity (κ_L). Because the carrier thermal conductivity can be calculated by the Wiedemann−Franz law, $\kappa_e = L_0 \sigma T$, where L_0 and σ are the Lorenz number and the electrical conductivity, respectively; the lattice thermal conductivity can also be estimated. Consequently, the figures of merit for all samples were calculated using the following equation: $ZT = \alpha^2 \sigma T/\kappa$.

3. RESULTS AND DISCUSSION

In a previous report, we presented a method for obtaining a reactive bismuth source (Bi^{3+} ions) from a bismuth precursor, bismuth nitrate ($Bi(NO_3)_3$), which could then be reacted with anions (e.g., Te^{2-}) to obtain a Bi_2Te_3-type nanomaterial.[45−47,49] Unlike most nitrate-type metal salts, $Bi(NO_3)_3$ does not dissolve in aqueous solutions but is easily hydrolyzed to form bismuth(III) hydroxide ($Bi(OH)_3$) (eq 1). Because of the extensive precipitation of $Bi(OH)_3$, it is impossible to

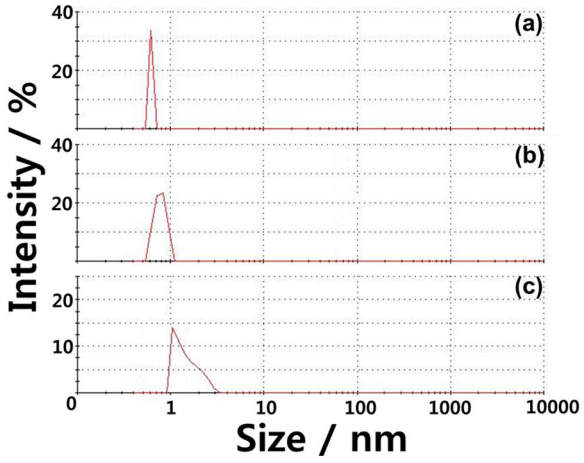

Figure 1. Size distribution of bismuth sources prepared at various pH levels; the distributions were obtained from dynamic light scattering (DLS) analysis: (a) pH 5.5, (b) 9.5, and (c) 12.5.

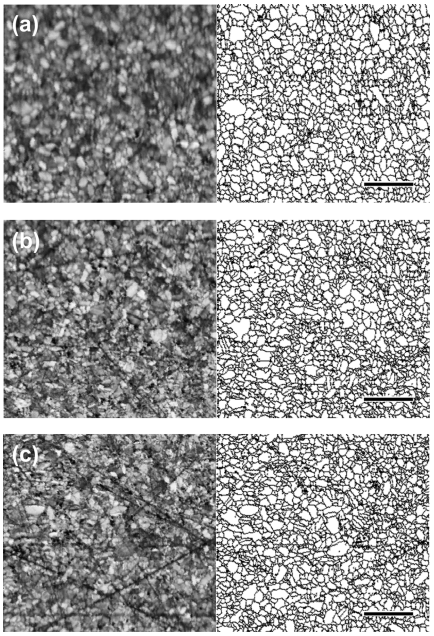

Figure 2. Electron backscatter diffraction (EBSD) images for the sintered specimens prepared at various pH levels: (a) 5.5, (b) 9.5, and (c) 12.5. The images for each specimen were subdivided into image-quality maps (left) and blank maps (right). The scale bar is 10 μm.

synthesize the desired nanomaterial in aqueous solutions without adopting a complementary treatment. We attempted to dissolve $Bi(OH)_3$ precipitates using a reducing agent. Inorganic reducing agents, such as hydrazine hydrate (N_2H_4) and sodium borohydride ($NaBH_4$), which are commonly used for the reduction of metal ions or metal oxides, have sufficient reducing power to convert $Bi(OH)_3$ directly to bismuth particles (Bi^0); i.e., their standard reduction potentials (eqs 2 and 3) are substantially lower than that of $Bi(OH)_3$ (eq 4),[50,51] and the reaction in eq 4 therefore occurs spontaneously when they are used. This reduction of $Bi(OH)_3$ (eq 4) was regarded as an undesired reaction because the resulting bismuth particles may not react with the anions.

$$Bi(NO_3)_3\ (s) + 3H_2O\ (l) \rightarrow Bi(OH)_3\ (s) \downarrow + 3H^+ + 3NO_3^- \quad (1)$$

$$N_2H_4 + 4OH^- \rightarrow N_2 + 4H_2O + 4e^-, \quad E^\circ = -1.16\ V \quad (2)$$

$$BH_4^- + 8OH^- \rightarrow BO_2^- + 6H_2O + 8e^-, \quad E^\circ = -1.24\ V \quad (3)$$

$$Bi(OH)_3 + 3e^- \rightarrow Bi + 3OH^-, \quad E^\circ = -0.46\ V \quad (4)$$

Instead of using reducing agents, we selected an appropriate organic reagent to dissolve the $Bi(OH)_3$ precipitates because some organic compounds exhibit relatively mild reducing power[52] and might limit the direct reduction of $Bi(OH)_3$. We chose ascorbic acid because of its easily tunable pH-dependent reducing power.

$$C_6H_8O_6 \rightarrow C_6H_6O_6 + 2H^+ + 2e^-, \quad E^\circ = 0.08\ V$$

$$E = E^\circ - 0.059pH \quad (5)$$

The effect of pH on the reducing power of ascorbic acid has been clearly defined.[52] As presented in eq 5, the reduction potential of ascorbic acid decreases with increasing pH, which indicates an enhancement of its reducing power. Adjustment of the pH to control the reduction potential of ascorbic acid enabled the reduction of $Bi(OH)_3$. The reduction potential of ascorbic acid ($E = E^\circ - 0.059pH$, eq 5) must be greater than that of $Bi(OH)_3$ (−0.46 V, eq 4) to prevent the direct reduction of $Bi(OH)_3$. On the basis of this criterion, the pH should be lower than ca. 9.2. In our previous work, we maintained the pH at 11, and the reduction potential of ascorbic acid (−0.57 V) decreased to less than that of $Bi(OH)_3$ (−0.46 V), which resulted in the direct reduction of $Bi(OH)_3$. We expected that some amount of $Bi(OH)_3$ might be converted into bismuth particles because the A solution became brown at pH 11 (see Experimental Section). The bismuth particles did not react with anions (Te^{2-}/Se^{2-}) at pH 11 and were possibly removed during filtering or washing steps, which led to insufficient bismuth content in the final product. We recovered the removed bismuth particles to confirm their oxidation state via XPS analysis (Supporting Information, Figure S1). When the pH is maintained at a level less than 9.2, the reduction potential of ascorbic acid is greater than that of $Bi(OH)_3$, and the direct reduction of $Bi(OH)_3$ to bismuth particles decreases. Consequently, ascorbic acid primarily causes the dehydrolysis of $Bi(OH)_3$, as shown in eq 6, and the reactive bismuth source, Bi^{3+} ion, is obtained.

$$Bi(OH)_3 + 3H^+ \rightarrow Bi^{3+} + H_2O \quad (6)$$

$$Te + 2e^- \rightarrow Te^{2-}, \quad E^\circ = -1.14\ V \quad (7a)$$

$$Se + 2e^- \rightarrow Se^{2-}, \quad E^\circ = -0.92\ V \quad (7b)$$

To synthesize $Bi_2Te_{2.7}Se_{0.3}$ nanomaterials, we preferentially reduced tellurium and selenium (Te/Se) using $NaBH_4$. The reactive anions (Te^{2-}/Se^{2-}) could be easily obtained because the reduction potentials of Te and Se (eqs 7a and 7b) are greater than that of $NaBH_4$ (eq 3). When Te and Se elements are reduced by $NaBH_4$ in an alkaline aqueous solution, the proposed mechanisms for the reduction can be described as follows:[45]

Table 1. Atomic Ratios of Specimens Prepared at Various pH Levels[a]

		Bi			Te			Se		
		concen.			concen.			concen.		
sample	no.	mg L^{-1}	mmol L^{-1}	at. ratio	mg L^{-1}	mmol L^{-1}	at. ratio	mg L^{-1}	mmol L^{-1}	at. ratio
pH 5.5	1	329.8	1.578	2.01	270.1	2.117	2.70	19.0	0.241	0.31
	2	332.2	1.590	2.01	273.1	2.140	2.70	19.5	0.247	0.31
	3	330.5	1.581	2.01	271.7	2.129	2.70	18.9	0.239	0.30
	ave.	330.8	1.583	2.01	271.6	2.129	2.70	19.1	0.242	0.31
pH 9.5	1	339.7	1.626	1.94	288.1	2.258	2.70	20.3	0.257	0.31
	2	341.5	1.634	1.94	289.5	2.269	2.70	19.8	0.251	0.30
	3	338.5	1.620	1.92	290.1	2.274	2.70	20.1	0.255	0.30
	ave.	339.9	1.626	1.94	289.2	2.267	2.70	20.1	0.254	0.30
pH 12.5	1	308.7	1.477	1.90	267.6	2.097	2.70	18.7	0.237	0.30
	2	309.1	1.479	1.90	268.5	2.104	2.70	18.8	0.238	0.31
	3	309.7	1.482	1.90	269.1	2.109	2.70	19.1	0.242	0.31
	ave.	309.2	1.479	1.90	268.4	2.103	2.70	18.9	0.239	0.31

[a]The chemical compositions were evaluated using inductively coupled plasma mass spectrometry (ICP-MS). The tellurium ratio was chosen as a reference point.

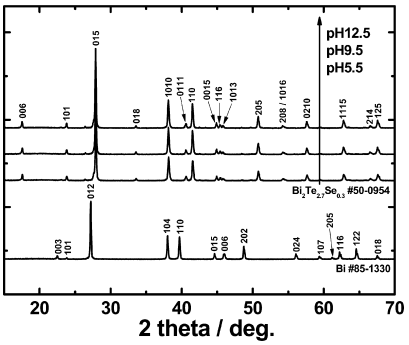

Figure 3. Comparison of XRD patterns between a commercial elemental bismuth and the specimens prepared at different pH levels.

$$3Te + 6OH^- \rightarrow 2Te^{2-} + TeO_3^{2-} + 3H_2O \quad (8)$$

$$2TeO_3^{2-} + NaBH_4 \rightarrow Te^{2-} + Te + NaBO_3 + H_2O + 2OH^- \quad (9)$$

$$5Te + 10OH^- + NaBH_4 \rightarrow 5Te^{2-} + NaBO_3 + 7H_2O \quad (10)$$

Commercial tellurium powder can be dissolved in an alkaline aqueous solution to yield Te^{2-} and TeO_3^{2-} ions (eq 8). $NaBH_4$ reduces TeO_3^{2-} ions to Te^{2-} and Te (eq 9). The newly produced Te easily produces Te^{2-} through the disproportionation (eq 8) under the alkaline condition. The overall reaction for Te reduction can be expressed as eq 10. We consider that selenium undergoes the same reducing mechanisms (eqs 11, 12, and 13).

$$3Se + 6OH^- \rightarrow 2Se^{2-} + SeO_3^{2-} + 3H_2O \quad (11)$$

$$2SeO_3^{2-} + NaBH_4 \rightarrow Se^{2-} + Se + NaBO_3 + H_2O + 2OH^- \quad (12)$$

$$5Se + 10OH^- + NaBH_4 \rightarrow 5Se^{2-} + NaBO_3 + 7H_2O \quad (13)$$

We assumed that Bi^{3+} ions were mostly formed at pH levels between 3 and 5 because colorless transparent A solutions were obtained in this pH range (see Experimental Section); i.e., Bi^{3+} ions were mainly generated when the A solution was acidic, whereas the amount of bismuth particles evidently increased as the A solution was made basic. The A solution should be maintained under slightly acidic conditions for the reaction of Bi^{3+} ions with anions (Te^{2-}/Se^{2-}). We adjusted the pH of the A solution from acidic to basic conditions to prepare various bismuth sources. We thoroughly examined the effect of pH on these sources, which were individually reacted with anions to prepare $Bi_2Te_{2.7}Se_{0.3}$ nanomaterials (eq 14). We closely observed the variation in the stoichiometry of these nanomaterials when different bismuth sources were used.

$$2Bi^{3+} + 2.7Te^{2-} + 0.3Se^{2-} \rightarrow Bi_2Te_{2.7}Se_{0.3} \quad (14)$$

By considering the criterion point of pH (i.e., pH 9.2), where the reduction potential of ascorbic acid ($E = E^\circ - 0.059$pH, eq 5) is equivalent to that of $Bi(OH)_3$ (−0.46 V), we preferentially prepared an A solution with a pH of 9.5. We also prepared A solutions with pH values of 5.5 and 12.5 to investigate the effect of pH on the bismuth sources (see Experimental Section). According to the DLS results in Figure 1, the particle size and the particle size distribution increased and broadened, respectively, as the pH was increased. Because the reduction potential of ascorbic acid at pH 5.5 (−0.24 V) was greater than that of $Bi(OH)_3$ (−0.46 V), the direct reduction of $Bi(OH)_3$ (eq 4) was strongly suppressed, whereas the dehydrolysis of $Bi(OH)_3$ (eq 6) was promoted. Accordingly, Bi^{3+} ions were preferentially formed instead of bismuth particles at pH 5.5, which may explain the relatively small particle size and narrow size distribution (Figure 1a). Meanwhile, the reduction potential of ascorbic acid at pH 9.5 (−0.48 V) decreased to less than that of $Bi(OH)_3$ (−0.46 V), and bismuth particles may have thus been generated, thereby resulting in somewhat larger particle sizes and a broader size distribution (Figure 1b). The reduction of $Bi(OH)_3$ should be accelerated at pH 12.5, such that the amount of bismuth particles might increase in the A solution and an even larger particle size and distribution may appear, as shown in Figure 1c.

The three different A solutions were individually reacted with Te^{2-}/Se^{2-} ions, and the resulting powders were sintered via an SPS process. According to the EBSD analyses for the sintered specimens, all of the specimens were composed of grains with an average size of ca. 0.5−1.5 μm. Besides, the grain size

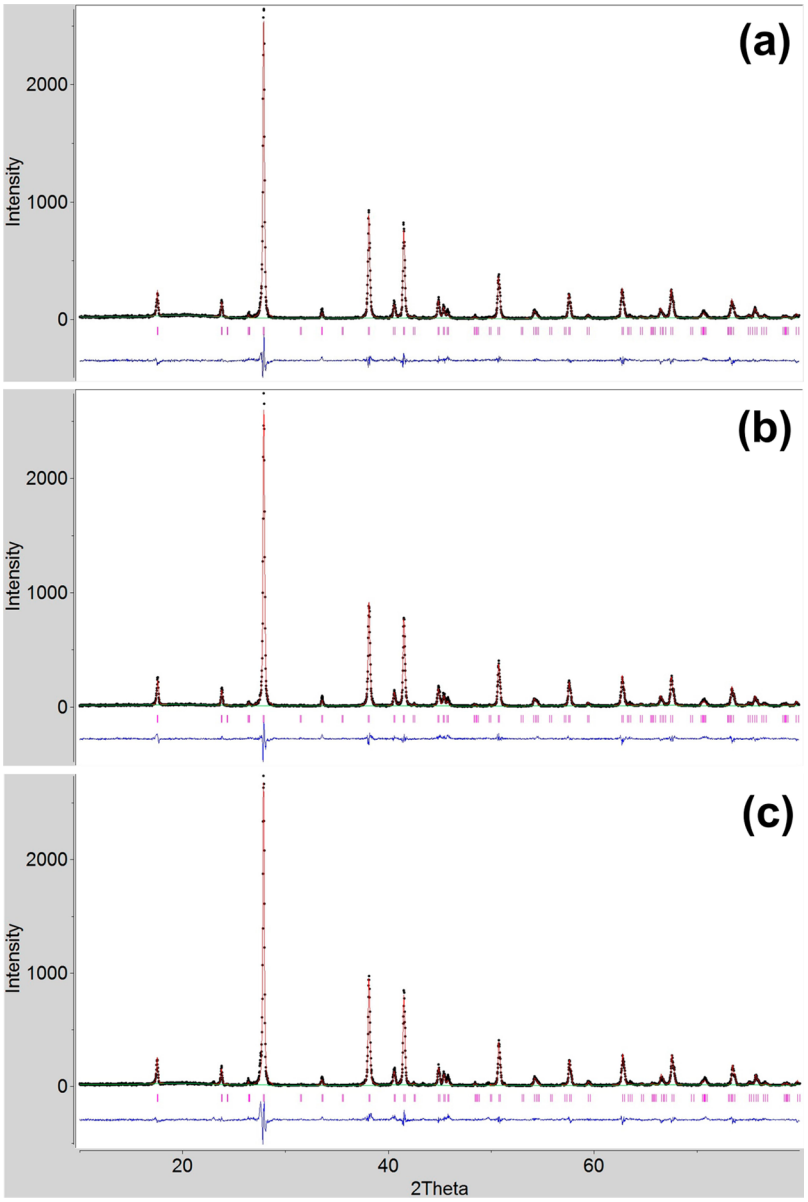

Figure 4. X-ray Rietveld refinement profiles for the specimens prepared at different pH levels: (a) 5.5, (b) 9.5, and (c) 12.5. Each image contains the observed (black dots), calculated (red line), and difference profile (blue line) as the refined pattern of the specimen.

Table 2. Final Rietveld Refinement Results for the Specimens Prepared at Different pH Levels

sample	a/Å	c/Å	V/Å^3	R_p	R_{wp}	reduced χ^2
pH 5.5	4.3493	30.2855	496.139	11.42	16.41	1.321
pH 9.5	4.3490	30.2843	496.044	10.61	15.90	1.178
pH 12.5	4.3469	30.2699	495.335	12.61	17.78	1.609

seemed to be independent of the pH variation (Figure 2). We conducted a quantitative analysis (ICP-MS) for the sintered specimens. The bismuth ratio was somewhat less than the desired ratio at pH 9.5 (Table 1) because some bismuth particles were generated instead of Bi^{3+} ions due to the lower reduction potential of ascorbic acid (−0.48 V) compared to that of $Bi(OH)_3$ (−0.46 V). These particles did not react with the anions. We assumed that the bismuth particles were removed during the filtering or washing steps. More bismuth

Table 3. Variation in the Thermoelectric Transport Properties of $Bi_2Te_{2.7}Se_{0.3}$ at 25°C as a Function of pH in the Preparation of Bismuth Sources

sample	carrier concentration/ 10^{19} cm^{-3}	carrier mobility/ cm^2 V^{-1}s^{-1}	resistivity/ $\mu\Omega$ m	Seebeck coefficient/ μV K^{-1}	power factor/ mW m^{-1}K^{-2}	thermal conductivity/ W m^{-1}K^{-1}
pH 5.5	3.12	176	11.4	−178	2.78	1.01
pH 9.5	4.10	154	9.90	−154	2.39	1.17
pH 12.5	5.85	130	8.20	−126	1.93	1.27

dx.doi.org/10.1021/am405035z | ACS Appl. Mater. Interfaces 2014, 6, 778−785

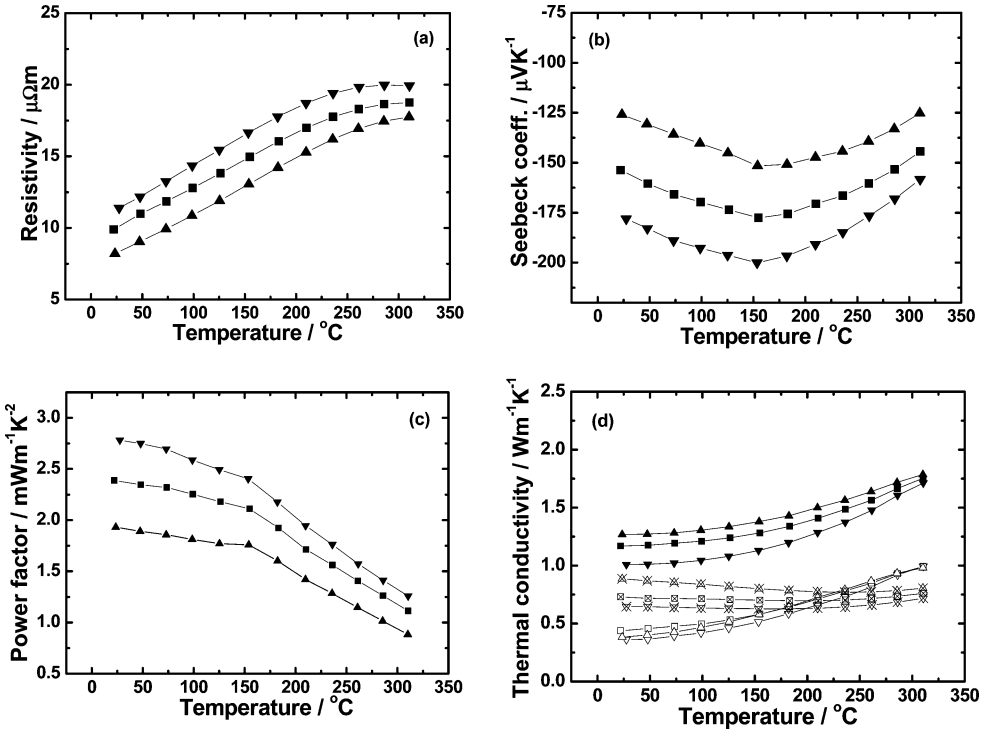

Figure 5. The effect of pH (5.5 (▼, ▽, ▽ with an × through it), 9.5 (■, □, □ with an × through it), and 12.5 (▲, △, △ with an × through it)) on thermoelectric transport properties of $Bi_2Te_{2.7}Se_{0.3}$: resistivity (a), Seebeck coefficient (b), power factor (c), and total thermal conductivity divided into lattice (κ_L-▽, □, △) and carrier (κ_e-▽ with an × through it, □ with an × through it, △ with an × through it) terms (d).

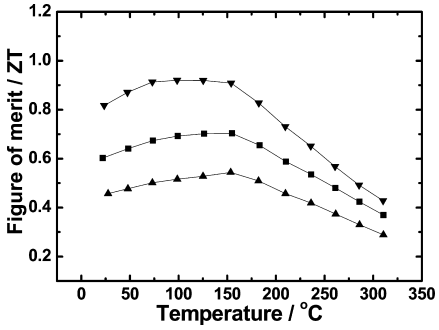

Figure 6. Figures of merit for $Bi_2Te_{2.7}Se_{0.3}$ prepared at various pH levels: 5.5 (▼), 9.5 (■), and 12.5 (▲).

particles were generated at pH 12.5 because of the even lower reduction potential of ascorbic acid (−0.66 V); thus, the bismuth ratio was far less than the desired ratio (Table 1). In contrast, the desired bismuth ratio was achieved at pH 5.5, presumably because the high reduction potential of ascorbic acid (−0.24 V) precluded the direct reduction of $Bi(OH)_3$ and caused its dehydrolysis. Therefore, Bi^{3+} ions may have been sufficiently supplied to the reaction, with the formation of almost no bismuth particles. According to the XRD result for the specimens shown in Figure 3, a single phase of $Bi_2Te_{2.7}Se_{0.3}$ rhombohedral structure (JCPDS Card No. 50-0954) was maintained regardless of the variation in pH; any possible second phase such as an elemental bismuth (trigonal structure, JCPDS Card No. 85-1330) was not detected. The diffraction results were refined by the Rietveld method; the X-ray Rietveld refinement profiles are shown in Figure 4 while lattice parameters from the structure refinement are given in Table 2. The lattice parameters gradually decrease as pH increases, and this clearly indicates unit cell contraction. Similar tendency was also observed when we attempted to calculate lattice parameters via the plane-spacing equation for a hexagonal crystal structure (Supporting Information, Table S1). We consider that the contraction should be caused by the decrease in bismuth composition with pH increase (Table 1). As no second phase was detected in both the diffraction patterns and the Rietveld refinement profiles while bismuth deficiency was observed in the ICP result, we assume that bismuth-deficient nonstoichiometric compounds were generated as pH increased.

Because the pH strongly influenced the bismuth ratios in the final products, their carrier concentrations were also affected by pH: as pH decreased, the bismuth ratio gradually increased (Table 1), the carrier concentration decreased, and the Seebeck coefficient increased (Table 3). The carrier mobility decreased as pH increased. It is possibly because a sodium residue from the pH controller (i.e., NaOH) might rest in the sample and the residue suppressed carrier mobility. The carrier mobility does not seem to be seriously repressed at pH 5.5, but it should greatly be restrained at higher pH values. Although the carrier mobility increased as pH decreased, electrical resistivity increased because the effect of the decrease in carrier concentration should be greater. Despite the increase of electrical resistivity, the power factor increased because the rate of increase in the Seebeck coefficient was greater than the rate of increase in electrical resistivity (Figure 5a,b). The power factor gradually increased as the pH was adjusted to weakly acidic conditions. The maximum power factor was obtained at a pH of 5.5 (Figure 5c).

The thermal conductivity also dependent on pH (Table 3). The total thermal conductivity is roughly the sum of the lattice and the carrier thermal conductivities.[45] We estimated the lattice term by calculating the carrier term through Wiedemann−Franz law. It was confirmed that the lattice thermal conductivity was barely affected by the pH variation

dx.doi.org/10.1021/am405035z | ACS Appl. Mater. Interfaces 2014, 6, 778−785

(Figure 5d). It is generally known that lattice thermal conductivity is affected by various phonon scattering mechanisms, such as phonon−phonon scattering, phonon−electron scattering, phonon−impurity scattering, phonon−defect scattering, and phonon−boundary scattering.[16] Considering that the lattice thermal conductivity was almost constant, the pH variation seems to cause none of the phonon scatterings. In contrast, the carrier term varied, possibly because of fluctuations in the carrier concentration caused by the variation in pH. The carrier concentration decreased with decreasing pH (Table 3); thus, the carrier term should have also decreased (Figure 5d). The decrease in the carrier term might reduce the total thermal conductivity. The figure of merit (ZT) was expected to depend on both the power factor and the thermal conductivity, which fluctuated with pH. When we optimized both the power factor and the thermal conductivity at pH 5.5, the ZT was maximized to 0.82 at 25 °C and 0.92 at 100 °C (Figure 6).

On the basis of theoretical reaction mechanisms, we attempted to manipulate the reaction conditions to regulate the stoichiometry of $Bi_2Te_{2.7}Se_{0.3}$ nanomaterials. As previously discussed, we obtained a reactive bismuth source (i.e., Bi^{3+} ions) through the simple manipulation of pH. By reacting the bismuth source with anions (Te^{2-}/Se^{2-}), we obtained nanomaterials with the desired stoichiometry. We optimized the thermoelectric transport properties with the desired stoichiometry, which maximized the ZT value.

4. CONCLUSIONS

We fabricated ternary n-type bismuth tellurium selenide nanomaterials for thermoelectric applications via a water-based chemical reaction under an atmospheric environment. In this work, bismuth nitrate was used as a bismuth precursor and was hydrolyzed to form bismuth hydroxide. The bismuth hydroxide was dissolved using ascorbic acid to give a reactive bismuth source (i.e., Bi^{3+} ions). The amount of Bi^{3+} ions, which reacted with anions (Te^{2-}/Se^{2-}), varied with pH; thus, the bismuth content in the nanomaterial varied with pH. We confirmed that the stoichiometry of the nanomaterial could be adjusted through a simple alteration of the pH with a concomitant variation of the thermoelectric transport properties. We optimized the transport properties by regulating the pH and thus maximized the thermoelectric performance.

■ ASSOCIATED CONTENT

Supporting Information

XPS spectra for the bismuth particle obtained from the conducted reaction and for a commercial bismuth element. The lattice parameters of products, calculated by using the plane-spacing equation combined with the Bragg's law. This information is available free of charge via the Internet at http://pubs.acs.org/.

■ AUTHOR INFORMATION

Corresponding Authors

*Tel.: +82-53-785-3600. Fax: +82-53-785-3609. E-mail: hoykim@dgist.ac.kr (H. Kim).

*Tel.: +82-53-785-3602. Fax: +82-53-785-3609. E-mail: charming0207@dgist.ac.kr (C. Kim).

Notes

The authors declare no competing financial interest.

■ ACKNOWLEDGMENTS

This work was financially supported by the DGIST R & D Program of the Ministry of Science, ICT, and Future Planning (MSIP) of Korea. We specially thank Prof. Seung-Tae Hong in DGIST for the technical support for the Rietveld analyses.

■ REFERENCES

(1) Chen, Z. G.; Han, G.; Yang, L.; Cheng, L.; Zou, J. *Prog. Nat. Sci.* **2012**, *22*, 535−549.

(2) Dresselhaus, M. S.; Chen, G.; Tang, M. Y.; Yang, R. G.; Lee, H.; Wang, D. Z.; Ren, Z. F.; Fleurial, J. P.; Gogna, P. *Mater. Res. Soc. Symp. Proc.* **2005**, *886*, 0886-F01-01.

(3) Byrnes, D. F.; Heshmatpour, B. *Mater. Res. Soc. Symp. Proc.* **2005**, *886*, 0886-F12-03.

(4) Tritt, T. M.; Zhang, B.; Gothard, N.; He, J.; Ji, X.; Thompson, D.; Kolis, J. W. *Mater. Res. Soc. Symp. Proc.* **2005**, *886*, 0886-F02-01.

(5) Sootsman, J.; Kong, H.; Uher, C.; Downey, A.; D'Angelo, J. J.; Wu, C.-I.; Hogan, T.; Caillat, T.; Kanatzidis, M. *Mater. Res. Soc. Symp. Proc.* **2007**, *1044*, 1044-U08-01.

(6) Hsu, K. F.; Loo, S.; Guo, F.; Chen, W.; Dyck, J. S.; Uher, C.; Hogan, T.; Polychroniadis, E. K.; Kanatzidis, M. G. *Science* **2004**, *303*, 818−821.

(7) Ji, X.; Zhang, B.; Tritt, T. M.; Kolis, J. W.; Kumbhar, A. *J. Electron. Mater.* **2007**, *36*, 721−726.

(8) Bell, L. E. *Science* **2008**, *321*, 1457−1461.

(9) Dresselhaus, M. S.; Chen, G.; Tang, M. Y.; Yang, R. G.; Lee, H.; Wang, D. Z.; Ren, Z. F.; Fleurial, J. P.; Gogna, P. *Adv. Mater.* **2007**, *19*, 1043−1053.

(10) Snyder, G. J.; Toberer, E. S. *Nat. Mater.* **2008**, *7*, 105−114.

(11) Zhu, T. J.; Liu, Y. Q.; Zhao, X. B. *Mater. Res. Bull.* **2008**, *43*, 2850−2854.

(12) Rey, A.; Faraldos, M.; Casas, J. A.; Zazo, J. A.; Bahamonde, A.; Rodríguez, J. J. *Key Eng. Mater.* **2008**, *368*−*372*, 550−552.

(13) Martin, J.; Nolas, G. S.; Zhang, W.; Chen, L. *Appl. Phys. Lett.* **2007**, *90*, 222112.

(14) Rowe, D. W. *Thermoelectrics Handbook: Macro to Nano*; CRC/Taylor & Francis: Boca Raton, 2006.

(15) Kurosaki, K.; Matsuda, T.; Uno, M.; Kobayashi, S.; Yamanaka, S. *J. Alloys Compd.* **2001**, *319*, 271−275.

(16) Goldsmid, H. J. *Introduction to Thermoelectricity*; Springer: Berlin, 2009.

(17) Peng, J.; He, J.; Alboni, P. N.; Tritt, T. M. *J. Electron. Mater.* **2009**, *38*, 981−984.

(18) Nolas, G. S.; Morelli, D. T.; Tritt, T. M. *Annu. Rev. Mater. Sci.* **1999**, *29*, 89−116.

(19) Min, G.; Rowe, D. M. *J. Mater. Sci. Lett.* **1999**, *18*, 1305−1306.

(20) Grytsiv, A.; Rogl, P.; Berger, S.; Paul, C.; Michor, H.; Bauer, E.; Hilscher, G.; Godart, C.; Knoll, P.; Musso, M.; Lottermoser, W.; Saccone, A.; Ferro, R.; Roisnel, T.; Noel, H. *J. Phys.: Condens. Matter* **2002**, *14*, 7071−7090.

(21) Tang, J.; Rachi, T.; Kumashiro, R.; Avila, M. A.; Suekuni, K.; Takabatake, T.; Guo, F. Z.; Kobayashi, K.; Akai, K.; Tanigaki, K. *Phys. Rev. B* **2008**, *78*, 085203.

(22) Hermann, R. P.; Grandjean, F.; Keppens, V.; Schweika, W.; Nolas, G. S.; Mandrus, D. G.; Sales, B. C.; Christen, H. M.; Bonville, P.; Long, G. J. *Mater. Res. Soc. Symp. Proc.* **2005**, *886*, 0886-F10-01.

(23) Paschen, S.; Pacheco, V.; Bentien, A.; Sanchez, A.; Cabrera, W. C.; Baenitz, M.; Iversen, B. B.; Grin, Y.; Steglich, F. *Phys. B* **2003**, *328*, 39−43.

(24) Shiohara, A.; Hanada, S.; Prabakar, S.; Fujioka, K.; Lim, T. H.; Yamamoto, K.; Northcote, P. T.; Tilley, R. D. *J. Am. Chem. Soc.* **2010**, *132*, 248−253.

(25) Ruberu, T. P. A.; Albright, H. R.; Callis, B.; Ward, B.; Cisneros, J.; Fan, H. J.; Vela, J. *ACS Nano* **2012**, *6*, 5348−5359.

(26) Wang, Z.; Shakya, A.; Gu, J.; Lian, S.; Maldonado, S. *J. Am. Chem. Soc.* **2013**, *135*, 9275−9278.

(27) Vaidyanathan, R.; Cox, S. M.; Happek, U.; Banga, D.; Mathe, M. K.; Stickney, J. L. *Langmuir* **2006**, *22*, 10590−10595.

(28) Hu, M.; Poulikakos, D. *Nano Lett.* **2012**, *12*, 5487−5494.
(29) Deng, Y.; Zhou, X.; Wei, G.; Liu, J.; Nan, C. W.; Zhao, S. *J. Phys. Chem. Solids* **2002**, *63*, 2119−2121.
(30) Ji, X.; Zhao, X.; Zhang, Y.; Lu, B.; Ni, H. *Mater. Res. Soc. Symp. Proc.* **2004**, *793*, S1.4.
(31) Poudel, B.; Hao, Q.; Ma, Y.; Lan, Y.; Minnich, A.; Yu, B.; Yan, X.; Wang, D.; Muto, A.; Vashaee, D.; Chen, X.; Liu, J.; Dresselhaus, M. S.; Chen, G.; Ren, Z. *Science* **2008**, *320*, 634−638.
(32) Zhao, X. B.; Ji, X. H.; Zhang, Y. H.; Zhu, T. J.; Tu, J. P.; Zhang, X. B. *Appl. Phys. Lett.* **2005**, *86*, 062111.
(33) Hone, J.; Ellwood, I.; Muno, M.; Mizel, A.; Cohen, M. L.; Zettl, A.; Rinzler, A. G.; Smalley, R. E. *Phys. Rev. Lett.* **1998**, *80*, 1042−1045.
(34) Cao, Y. Q.; Zhu, T. J.; Zhao, X. B. *J. Alloys Compd.* **2008**, *449*, 109−112.
(35) Lu, J.; Han, Q.; Yang, X.; Lu, L.; Wang, X. *Mater. Lett.* **2007**, *61*, 3425−3428.
(36) Zhao, X. B.; Ji, X. H.; Zhang, Y. H.; Lu, B. H. *J. Alloys Compd.* **2004**, *368*, 349−352.
(37) Sun, T.; Zhao, X. B.; Zhu, T. J.; Tu, J. P. *Mater. Lett.* **2006**, *60*, 2534−2537.
(38) Xie, W.; Tang, X.; Yan, Y.; Zhang, Q.; Tritt, T. M. *Appl. Phys. Lett.* **2009**, *94*, 102111.
(39) Cao, Y. Q.; Zhao, X. B.; Zhu, T. J.; Zhang, X. B.; Tu, J. P. *Appl. Phys. Lett.* **2008**, *92*, 143106.
(40) Nolas, G. S.; Sharp, J.; Goldsmid, H. J. *Thermoelectrics: Basic Prinsicples and New Materials Developments*; Springer: Berlin, 2001.
(41) Fleurial, J. P.; Gailliard, L.; Triboulet, R.; Scherrer, H.; Scherrer, S. *J. Phys. Chem. Solids* **1988**, *49*, 1237−1247.
(42) Lee, J. K.; Park, S. D.; Kim, B. S.; Oh, M. W.; Cho, S. H.; Min, B. K.; Lee, H. W.; Kim, M. H. *Electron. Mater. Lett.* **2010**, *6*, 201−207.
(43) Hicks, L. D.; Harman, T. C.; Sun, X.; Dresselhaus, M. S. *Phys. Rev. B* **1996**, *53*, R10493−R10496.
(44) Gu, Z.; Han, Y.; Pan, F.; Wang, X.; Weng, D.; Zhou, S. *Mater. Sci. Forum* **2009**, *610*−*613*, 394−398.
(45) Kim, C.; Kim, D. H.; Kim, J. S.; Han, Y. S.; Chung, J. S.; Kim, H. *J. Alloys Compd.* **2011**, *509*, 9472−9478.
(46) Kim, C.; Kim, D. H.; Kim, H.; Chung, J. S. *ACS Appl. Mater. Interfaces* **2012**, *4*, 2949−2954.
(47) Kim, C.; Kim, D. H.; Han, Y. S.; Chung, J. S.; Park, S. H.; Park, S.; Kim, H. *Mater. Res. Bull.* **2011**, *46*, 407−412.
(48) Larson, A. C.; Von Dreele, R. B. *GSAS: Report LAUR 86e748*; Los Alamos National Laboratory: Los Alamos, NM, 2000.
(49) Kim, C.; Kim, D. H.; Han, Y. S.; Chung, J. S.; Park, S. H.; Kim, H. *Powder Tech.* **2011**, *214*, 463−468.
(50) Park, J. W.; Chae, E. H.; Kim, S. H.; Lee, J. H.; Kim, J. W.; Yoon, S. M.; Choi, J.-Y. *Mater. Chem. Phys.* **2006**, *97*, 371−378.
(51) Hayes, P. C. *Process Principles in Minerals and Materials Production*; Hayes Publishing Co.: Brisbane, 1993.
(52) Songping, W. *Mater. Lett.* **2007**, *61*, 1125−1129.